INTERNATIONAL JOURNAL FOR NUMERICAL METHODS IN ENGINEERING
Int. J. Numer. Meth. Engng 2000; **00**:1–6 *Prepared using* nmeauth.cls *[Version: 2002/09/18 v2.02]*

A dual-primal FETI method for solving a class of fluid-structure interaction problems in the frequency domain

Jing Li[1,*], Charbel Farhat[2,3,4], Philip Avery[2], and Radek Tezaur [2]

[1] *Department of Mathematical Sciences, Kent State University, Kent, OH 44242, U.S.A.*
[2] *Department of Aeronautics and Astronautics, Stanford University, Stanford, CA 94305, U.S.A.*
[3] *Department of Mechanical Engineering, Stanford University, Stanford, CA 94305, U.S.A.*
[4] *Institute for Computational & Mathematical Engineering, Stanford University, Stanford, CA 94305, U.S.A.*

SUMMARY

The dual-primal finite element tearing and interconnecting method (FETI-DP) is extended to systems of linear equations arising from a finite element discretization for a class of fluid-structure interaction problems in the frequency domain. A preconditioned GMRES iteration is used to solve the linear equations for the Lagrange multipliers introduced on the subdomain boundaries to enforce continuity of the solution. The coupling between the fluid and the structure on the fluid-structure interface requires an appropriate choice of coarse level degrees of freedom in the FETI-DP algorithm to achieve fast convergence. Several choices are proposed and tested by numerical experiments on three-dimensional fluid-structure interaction problems in the mid-frequency regime that demonstrate the greatly improved performance of the proposed algorithm over the standard FETI-DP method.

KEY WORDS: fluid-structure interaction, FETI, domain decomposition

1. Introduction

Fluid-structure interaction (FSI) problems arise in many engineering applications, cf. [21]. In the structural acoustics the time harmonic vibration of an elastic structure immersed in a fluid and the surrounding acoustic field are studied in response to incident acoustic waves and/or external forces. The motion of the structure is modeled by the elasto-dynamic equations for the structural displacements, and the acoustic waves in the fluid are modeled by the Helmholtz equation for the fluid pressure. The structure and the fluid are coupled across the fluid-structure interface via the equilibrium of the force and the compatibility of the normal displacement.

*Correspondence to: Jing Li, Department of Mathematical Sciences, Kent State University, Kent, OH 44242, U.S.A.; E-mail: li@math.kent.edu

Contract/grant sponsor: National Science Foundation; contract/grant number: DMS-0612574

Contract/grant sponsor: Office of Naval Research; contract/grant number: N00014-05-1-0204-1

Received xx/xx/xxxx
Revised xx/xx/xxxx

Finite element methods have become a popular choice for solving the FSI problems, cf. [22] and the references therein. In the mid-frequency regime, the finite element models require fine meshes and as a result lead to large-scale systems of equations with millions of degrees of freedom. With the extreme demands placed by direct methods on computer resources for solving these large-scale systems of equations, a large segment of the computational structural mechanics community has shifted its attention from direct to iterative solution strategies. However, there are very few discussions of iterative methods in the literature for solving the systems of linear equations arising from the finite element discretization of the FSI problems.

Massively parallel computation becomes a necessity for higher-fidelity three-dimensional models with millions of degrees of freedom (dof). Domain decomposition methods have emerged as powerful equation solvers in the field of computational mechanics on both sequential and parallel computing platforms. Among the most successful domain decomposition methods, the dual-primal finite element tearing and interconnecting method (FETI-DP) [9, 10] has been proven numerically scalable for solving both second- and fourth-order problems. The FETI-DP method has been extended to FETI-DPH (H for Helmholtz) for solving indefinite elastic vibration problems and acoustic scattering problems. In FETI-DPH, plane wave augmentations are added in the coarse problem, which has been shown to be crucial to its performance in the medium frequency regime [11, 12, 6].

The FETI-DP method has been applied to the solution of FSI problems by Dey and Datta [5] and by Walsh *et al.* [23], where the standard selection of coarse level degrees of freedom in FETI-DP was used. Another variant of the FETI method known as FETI-H [13] has also been extended by Mandel [19] to solve FSI problems in the frequency domain. However, its performance is not satisfactory in three dimensions.

In this paper, the FETI-DPH method is extended to the vibro-acoustic FSI problems. Several choices of the coarse level primal variables in FETI-DPH are discussed. It is shown that the straightforward application of FETI-DPH to the coupled problem performs poorly, and that including the appropriate degrees of freedom on the fluid-structure interface in the coarse problem is essential for improving performance. Such modifications of FETI-DPH improve both the iteration count and CPU time substantially.

The remainder of this paper is organized as follows. The partial differential equations describing the FSI problems and the system of linear equations arising from their finite element discretization are discussed in Section 2. The original FETI-DPH method for solving indefinite elastic vibration problems and acoustic scattering problems are reviewed in Section 3. Extensions of the FETI-DPH method to the vibro-acoustic FSI problems are discussed in Section 4, where both compatible and incompatible fluid and structure meshes are considered. In Section 5, numerical experiments of solving three-dimensional FSI problems on parallel processors demonstrate the effectiveness of the proposed algorithm.

2. The vibro-acoustic fluid-structure interaction problem

A three-dimensional elastic structure is embedded in a three-dimensional ideal, compressible fluid; the fluid region is denoted by Ω_f, and the structure by Ω_e. The fluid pressure, represented

by p, is governed by the wave equation

$$\Delta p = \frac{1}{c_f^2}\,\frac{\partial^2 p}{\partial t^2}, \tag{1}$$

where c_f is the *speed of sound* in the fluid. The vibration of the elastic structure follows the Navier's displacement equation of motion

$$\mu\Delta\mathbf{u} + (\Lambda+\mu)\nabla(\nabla\cdot\mathbf{u}) = \rho_e\frac{\partial^2\mathbf{u}}{\partial t^2}, \tag{2}$$

where $\mathbf{u}$ represents the displacement of the structure, Λ and μ its Lamé moduli, and ρ_e its density.

Time harmonic solutions of the coupled FSI system for a given circular frequency ω are sought here, i.e., the solutions to (1) and (2) in the form $p(x,t) = p(x)e^{-i\omega t}$, and $\mathbf{u}(x,t) = \mathbf{u}(x)e^{-i\omega t}$, where $x \in \mathbb{R}^3$ represents the spatial coordinates. Then, the Helmholtz equation for the fluid pressure $p(x)$ follows from the wave equation (1),

$$-\Delta p - k^2\, p = 0 \quad \text{in} \quad \Omega_f, \tag{3}$$

where $k = \omega/c_f$ is the so called wavenumber, and the equation for the structural displacement $\mathbf{u}(x)$ becomes

$$-\mu\Delta\mathbf{u} - (\Lambda+\mu)\nabla(\nabla\cdot\mathbf{u}) - \rho_e\omega^2\mathbf{u} = 0 \quad \text{in} \quad \Omega_e. \tag{4}$$

In this paper, the scattering of an incident acoustic wave $p_{inc} = e^{ikd\cdot x}$ by an elastic structure and the response of the structure to the incident wave are considered as a particular model application, though the FETI-DPH extension presented in this work is by no means restricted to this application. Here, $d \in \mathbb{R}^3$ represents the direction of the incident wave. The interface between the fluid and the structure is denoted by Γ. The following two transmission conditions must be satisfied on Γ

$$\tau(\mathbf{u})\cdot\mathbf{n} = -(p+p_{inc})\,\mathbf{n}, \quad \text{on} \quad \Gamma, \tag{5}$$

$$\mathbf{u}\cdot\mathbf{n} = \frac{1}{\rho_f\omega^2}\frac{\partial(p+p_{inc})}{\partial n}, \quad \text{on} \quad \Gamma, \tag{6}$$

where $\mathbf{n}$ is the unit outer normal on the structure surface, $\tau(\mathbf{u})$ the stress tensor, and ρ_f the density of the fluid. Equation (5) represents the balance of forces — that is, the equilibrium of the pressure and traction normal to the structure surface — and (6) represents the compatibility of the normal displacements of the fluid and structure subsystems. The following simple local absorbing boundary condition on an artificial outer boundary Σ of the fluid region is used

$$\frac{\partial p}{\partial\nu} - ikp = 0 \quad \text{on} \quad \Sigma. \tag{7}$$

The finite element method is used to solve the FSI problem (3)–(7). Let $\mathbf{V}$ and Q be the finite element spaces for the structure displacement $\mathbf{u}(x)$ and the fluid pressure $p(x)$, respectively. The finite element solution $(\mathbf{u},p) \in (\mathbf{V},Q)$ satisfies the following variational equations

$$\begin{aligned}
\int_{\Omega_e}\{\Lambda(\nabla\cdot\mathbf{u})(\nabla\cdot\mathbf{v}) + 2\mu e(\mathbf{u}):e(\mathbf{v})\} - \omega^2\int_{\Omega_e}\rho_e\mathbf{u}\cdot\mathbf{v} + \int_\Gamma p\mathbf{v}\cdot\mathbf{n} &= -\int_\Gamma p_{inc}\mathbf{v}\cdot\mathbf{n},\\
\int_{\Omega_f}\nabla p\cdot\nabla q - k^2\int_{\Omega_f} pq + ik\int_\Sigma pq + \rho_f\omega^2\int_\Gamma q\mathbf{u}\cdot\mathbf{n} &= \int_\Sigma\frac{\partial p_{inc}}{\partial\mathbf{n}}q,
\end{aligned}$$

for all $(\mathbf{v}, q) \in (\mathbf{V}, Q)$, where $e(\mathbf{u})$ is the strain tensor, and

$$e(\mathbf{u}) : e(\mathbf{v}) = \sum_{i,j=1}^{3} e_{ij}(\mathbf{u}) e_{ij}(\mathbf{v}), \quad \text{with} \quad e_{ij}(\mathbf{u}) = \frac{1}{2}\left(\frac{\partial u_i}{\partial x_j} + \frac{\partial u_j}{\partial x_i}\right).$$

Defining matrices and right-hand side vectors corresponding to the terms in the variational problem by

$$\mathbf{u}^T K_e \mathbf{v} = \int_{\Omega_e} \Lambda(\nabla \cdot \mathbf{u})(\nabla \cdot \mathbf{v}) + 2\mu e(\mathbf{u}) : e(\mathbf{v}), \quad p^T K_f q = \int_{\Omega_f} \nabla p \cdot \nabla q,$$

$$\mathbf{u}^T M_e \mathbf{v} = \int_{\Omega_e} \rho_e \mathbf{u} \cdot \mathbf{v}, \quad p^T M_f q = \int_{\Omega_f} pq, \quad p^T M_\Sigma q = \int_{\Sigma} pq,$$

$$p^T C_\Gamma \mathbf{v} = \int_{\Gamma} p\mathbf{v} \cdot \mathbf{n}, \quad \mathbf{f}^T \mathbf{v} = -\int_{\Gamma} p_{inc} \mathbf{v} \cdot \mathbf{n}, \quad \text{and} \quad g^T q = \int_{\Sigma} \frac{\partial p_{inc}}{\partial \mathbf{n}} q,$$

the following system of linear equations for the finite element solution $(\mathbf{u}, p) \in (\mathbf{V}, Q)$ is obtained

$$\begin{bmatrix} K_e - \omega^2 M_e & C_\Gamma^T \\ \rho_f \omega^2 C_\Gamma & K_f - k^2 M_f + ikM_\Sigma \end{bmatrix} \begin{bmatrix} \mathbf{u} \\ p \end{bmatrix} = \begin{bmatrix} \mathbf{f} \\ g \end{bmatrix}. \tag{8}$$

In this paper, the same notation, e.g., $\mathbf{u}$, is used to denote both a finite element function and its vector of coefficients with respect to the finite element basis functions.

The FSI is represented by the block C_Γ in (8); without C_Γ, the problem is reduced to a separate acoustic scattering problem for the fluid and an elastic vibration problem for the structure. To compute the FSI block C_Γ, the fluid mesh and the structure mesh are assumed to be compatible and Γ is formed by the element faces on the fluid-structure interface. The construction of C_Γ for incompatible fluid and structure meshes is discussed in Section 4.2.1.

The system of linear equations (8) for the FSI problem is derived above for the case of a three-dimensional isotropic solid elastic structure embedded in a three-dimensional fluid. The same procedure can also be applied to derive a similar system of linear equations for different and more general structures, including those made up of plates and shells. This will change the underlying operator for the stiffness matrix K_e, but the algorithms presented here still apply.

The two diagonal blocks in (8) correspond to the structural displacement and to the fluid pressure, respectively. In general, they may have quite different scales, which makes the system matrix in (8) extremely ill-conditioned. Before an iterative method can be used to solve (8), a scaling of the variables to make the diagonal blocks of similar size is necessary. Denoting $\widetilde{\Lambda}$ an average of the Lamé moduli Λ and μ on each element of the structure, a scaled displacement and force are defined by

$$\widetilde{\mathbf{u}} = \sqrt{\rho_f \omega^2 \widetilde{\Lambda}}\, \mathbf{u}, \quad \text{and} \quad \widetilde{\mathbf{f}} = \sqrt{\rho_f \omega^2 / \widetilde{\Lambda}}\, \mathbf{f}.$$

Then, the system of linear equations (8) can be written equivalently as

$$\begin{bmatrix} A_e & C_w^T \\ C_w & A_f \end{bmatrix} \begin{bmatrix} \widetilde{\mathbf{u}} \\ p \end{bmatrix} = \begin{bmatrix} \widetilde{\mathbf{f}} \\ g \end{bmatrix}, \tag{9}$$

where

$$A_e = 1/\widetilde{\Lambda}\left(K_e - \omega^2 M_e\right), \quad A_f = K_f - k^2 M_f + ikM_\Sigma, \quad \text{and} \quad C_w = \sqrt{\rho_f \omega^2/\widetilde{\Lambda}}\, C_\Gamma.$$

Similar scalings have been considered in [19, 23].

Equation (9) is a coupled system for the scaled structure displacement and the fluid pressure. It is in general indefinite. In the mid-frequency regime, the finite element discretization requires fine meshes and therefore leads to large-scale system of equations, which makes the solution by a direct solver impractical. An extension of the FETI-DP algorithm for acoustic problems and elastic vibration problems, namely the FETI-DPH algorithm, has shown parallel scalability, cf. [11, 12, 6]. However, a straightforward application of the FETI-DPH algorithm to the FSI problem has not been successful, cf. [5]. In this paper, a further extension of the FETI-DPH method to the FSI system (9) is proposed. To this effect, a review of the FETI-DPH algorithm for the solution of indefinite problems is given next.

3. The FETI-DPH method for vibration and acoustic problems

The dual-primal finite element tearing and interconnecting method FETI-DP [9, 10] is a third-generation FETI [14] method developed for the fast, iterative, and parallel solution of systems of equations arising from finite element solution of second-order and fourth-order elliptic partial differential equations. When equipped with the Dirichlet preconditioner and an appropriate coarse problem, the condition number of the FETI-DP algorithm has been proven to be independent of the number of subdomains. It was also proven to grow only polylogarithmically with the size of the individual subdomain problem for both second-order and fourth-order systems, and in both two and three dimensions, cf. [20, 16]. The parallel scalability of the FETI-DP method has been demonstrated in practice for many complex structural mechanics and structural dynamics problems, cf. [9, 10, 2].

FETI-DPH is an extension of FETI-DP to a class of indefinite problems arising from, e.g., elastic vibration problems and acoustic problems [11, 12, 6]. Consider an indefinite system,

$$Ax = b, \tag{10}$$

where A, x, and b can be chosen as A_e, $\widetilde{\mathbf{u}}$, or $\widetilde{\mathbf{f}}$, or as A_f, p, and g, from (9), corresponding to solving a structural or a fluid problem, respectively.

Let the original computational domain be decomposed into N non-overlapping subdomains, Ω_s, $s = 1, 2, \cdots, N$, with matching interfaces $\Upsilon^{(s,q)} = \partial\Omega_s \bigcap \partial\Omega_q$. Let $\Upsilon = \bigcup_{s=1,q>s}^{s=N} \Upsilon^{(s,q)}$ denote the whole interface of this decomposition. Let also $A^{(s)}$, $x^{(s)}$, and $b^{(s)}$ denote the restrictions to subdomain Ω_s of A, x, and b, respectively.

Let Υ_c denote the set of "corner" nodes lying on the global interface Υ, and let $\Upsilon' = \Upsilon \backslash \Upsilon_c$. Here the standard corner nodes can be defined for two-dimensional problems as the beginning and end mesh nodes of the boundary between two subdomains (see Figure 1 for an illustration) or for three-dimensional problems as mesh nodes that touch more than three subdomains; for a more sophisticated corner selection method, see [17]. If in each subdomain Ω_s the unknowns are partitioned into global corner dof designated by the subscript c, and the "remaining" dof

designated by the subscript r, $A^{(s)}$, $x^{(s)}$ and $b^{(s)}$ can be partitioned as follows

$$A^{(s)} = \begin{bmatrix} A_{rr}^{(s)} & A_{rc}^{(s)} \\ A_{cr}^{(s)} & A_{cc}^{(s)} \end{bmatrix}, \qquad x^{(s)} = \begin{bmatrix} x_r^{(s)} \\ x_c^{(s)} \end{bmatrix} \qquad \text{and} \qquad b^{(s)} = \begin{bmatrix} b_r^{(s)} \\ b_c^{(s)} \end{bmatrix}. \tag{11}$$

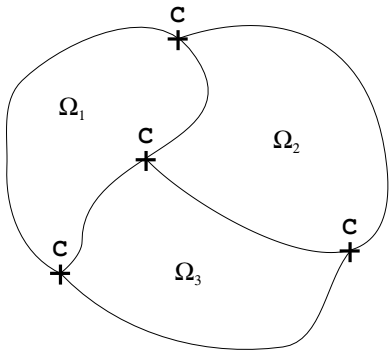

Figure 1. Example of a definition of corner points.

Let x_c denote the global vector of corner dof, and $x_c^{(s)}$ denote its restriction to Ω_s. Let also $B_r^{(s)}$ and $B_c^{(s)}$ be the two subdomain Boolean matrices defined by

$$B_r^{(s)} x_r^{(s)} = \pm x_r^{(s)} \qquad \text{and} \qquad B_c^{(s)} x_c = x_c^{(s)}, \tag{12}$$

where the $\pm$ sign is set by any convention such that $\sum_{s=1}^{N} B_r^{(s)} x_r^{(s)}$ represents the *jump* of x across the subdomain interfaces. Finally, let

$$b_c = \sum_{s=1}^{N} {B_c^{(s)}}^T b_c^{(s)}. \tag{13}$$

With these notations, problem (10) is equivalent to the following decomposed system

$$\begin{bmatrix} A_{rr}^{(1)} & \cdots & 0 & \widehat{A}_{rc}^{(1)} & {B_r^{(1)}}^T & {B_r^{(1)}}^T Q_b \\ \vdots & \ddots & \vdots & \vdots & \vdots & \vdots \\ 0 & \cdots & A_{rr}^{(N)} & \widehat{A}_{rc}^{(N)} & {B_r^{(N)}}^T & {B_r^{(N)}}^T Q_b \\ \widehat{A}_{cr}^{(1)} & \ldots & \widehat{A}_{cr}^{(N)} & \widehat{A}_{cc} & 0 & 0 \\ B_r^{(1)} & \ldots & B_r^{(N)} & 0 & 0 & 0 \\ Q_b^T B_r^{(1)} & \ldots & Q_b^T B_r^{(N)} & 0 & 0 & 0 \end{bmatrix} \begin{bmatrix} x_r^{(1)} \\ \vdots \\ x_r^{(N)} \\ x_c \\ \lambda \\ \mu \end{bmatrix} = \begin{bmatrix} b_r^{(1)} \\ \vdots \\ b_r^{(N)} \\ b_c \\ 0 \\ 0 \end{bmatrix}, \tag{14}$$

where $\widehat{A}_{cr}^{(s)} = {B_c^{(s)}}^T A_{cr}^{(s)}$, for $s = 1, 2, ..., N$, and $\widehat{A}_{cc} = \sum_{s=1}^{N} {B_c^{(s)}}^T A_{cc}^{(s)} B_c^{(s)}$. λ is the vector of Lagrange multipliers introduced on Υ' to enforce the continuity of the solution x

$$\sum_{s=1}^{N} B_r^{(s)} x_r^{(s)} = 0. \tag{15}$$

μ is another set of Lagrange multipliers introduced to enforce the optional continuity constraint

$$Q_b^T \sum_{s=1}^{N} B_r^{(s)} x_r^{(s)} = 0. \tag{16}$$

This optional constraint, whose concept was first developed in [7], is determined by a matrix Q_b with columns defined on Υ'. The word "optional" refers to the fact that (16) and the vector of Lagrange multipliers μ are not necessarily needed for formulating the above decomposed problem; the continuity constraints (15) imply (16) for any matrix Q_b. The purpose of applying the optional constraint is to enforce at each iteration the jump of the solution across the subdomain boundaries to be orthogonal to the columns of Q_b, which is crucial for the numerical scalability of the FETI-DP method in many applications.

By denoting

$$x_r = \begin{bmatrix} x_r^{(1)} \\ \vdots \\ x_r^{(N)} \end{bmatrix}, \quad A_{rr} = \begin{bmatrix} A_{rr}^{(1)} & \cdots & 0 \\ \vdots & \ddots & \vdots \\ 0 & \cdots & A_{rr}^{(N)} \end{bmatrix}, \quad b_r = \begin{bmatrix} b_r^{(1)} \\ \vdots \\ b_r^{(N)} \end{bmatrix}, \quad B_r = \begin{bmatrix} B_{rr}^{(1)} & \cdots & B_{rr}^{(N)} \end{bmatrix},$$

$$\widetilde{x}_c = \begin{bmatrix} x_c \\ \mu \end{bmatrix}, \quad \widetilde{A}_{cc} = \begin{bmatrix} \widehat{A}_{cc} & 0 \\ 0 & 0 \end{bmatrix}, \quad \widetilde{A}_{cr} = \begin{bmatrix} \widehat{A}_{cr}^{(1)} & \cdots & \widehat{A}_{cr}^{(N)} \\ Q_b^T B_r^{(1)} & \cdots & Q_b^T B_r^{(N)} \end{bmatrix}, \quad \widetilde{b}_c = \begin{bmatrix} b_c \\ 0 \end{bmatrix},$$

the decomposed problem (14) can be written in a compact form as follows

$$\begin{bmatrix} A_{rr} & \widetilde{A}_{rc} & B_r^T \\ \widetilde{A}_{cr} & \widetilde{A}_{cc} & 0 \\ B_r & 0 & 0 \end{bmatrix} \begin{bmatrix} x_r \\ \widetilde{x}_c \\ \lambda \end{bmatrix} = \begin{bmatrix} b_r \\ \widetilde{b}_c \\ 0 \end{bmatrix}. \tag{17}$$

Eliminating x_r and $\widetilde{x}_c$ from (17), the following interface problem for the Lagrange multipliers λ is obtained

$$(F_{rr} + \widetilde{F}_{rc} \widetilde{A}_{cc}^{*^{-1}} \widetilde{F}_{rc}^T)\lambda = d_r - \widetilde{F}_{rc} \widetilde{A}_{cc}^{*^{-1}} \widetilde{b}_c^*, \tag{18}$$

where

$$F_{rr} = B_r A_{rr}^{-1} B_r^T, \quad \widetilde{F}_{rc} = B_r A_{rr}^{-1} \widetilde{A}_{rc}, \quad \widetilde{A}_{cc}^* = \widetilde{A}_{cc} - \widetilde{A}_{cr} A_{rr}^{-1} \widetilde{A}_{rc},$$
$$d_r = B_r A_{rr}^{-1} b_r, \quad \text{and} \quad \widetilde{b}_c^* = \widetilde{b}_c - \widetilde{A}_{cr} A_{rr}^{-1} b_r. \tag{19}$$

When the system of linear equations (10) arises from the finite element discretization for elastic vibration problems or acoustic propagation problems, the resulting interface problem (18) is indefinite and a preconditioned GMRES iteration is used to solve (18). At each iteration, the matrix-vector product $(F_{rr} + \widetilde{F}_{rc} \widetilde{A}_{cc}^{*^{-1}} \widetilde{F}_{rc}^T)\lambda^n$ incurs the solution of a coarse problem of the form

$$\widetilde{A}_{cc}^* z = \widetilde{F}_{rc}^T \lambda^n. \tag{20}$$

The third equation of (19) shows that the size of this coarse problem is equal to the sum of the number of corner dof and the number of columns of Q_b.

For example, for three-dimensional symmetric positive definite problems, the columns of Q_b contain the translational rigid body modes on each edge of Υ', i.e., each three consecutive columns of Q_b are constructed as

$$\begin{aligned}
&[0\ \cdots\ 0\ \ [1\ 0\ 0\ \cdots\ 1\ 0\ 0\ \cdots\ 1\ 0\ 0]\ \ 0\ \cdots\ 0\ ]^T,\\
&[0\ \cdots\ 0\ \ [0\ 1\ 0\ \cdots\ 0\ 1\ 0\ \cdots\ 0\ 1\ 0]\ \ 0\ \cdots\ 0\ ]^T,\\
&[0\ \cdots\ 0\ \ [0\ 0\ 1\ \cdots\ 0\ 0\ 1\ \cdots\ 0\ 0\ 1]\ \ 0\ \cdots\ 0\ ]^T.
\end{aligned} \tag{21}$$

In (21), a block of the form 1 0 0 refers to the displacement at one interface node induced by a rigid body mode in the x direction, a block of the form 0 1 0 refers to the displacement induced by a rigid body mode in the y direction, and a block of the form 0 0 1 in the z direction. With such augmentation, the FETI-DP method equipped with the Dirichlet preconditioner is numerically scalable for the solution of three-dimensional second-order problems [16, 15].

However, the standard augmentation of rigid body modes is not sufficient to achieve scalable convergence rate for solving indefinite elastic vibration problems or acoustic propagation problems. Since the solutions of such problems represent wave propagation in the structure and in the fluid, respectively, it is intuitive to include traces of waves on Υ' in columns of Q_b. This idea has also been used in FETI-H for the Helmholtz equation [13].

The plane waves for the Helmholtz problem (3) are

$$v = \sum_{j=1}^{n_w} \left(\beta_j \sin(k\theta_j \cdot X) + \gamma_j \cos(k\theta_j \cdot X)\right), \tag{22}$$

where $X \in \mathbb{R}^3$ denotes the spatial coordinates, $\theta_j \in \mathbb{R}^3$ is a unit vector defining the direction of propagation of the plane wave, β_j and γ_j are any real coefficients, and n_w corresponds to the number of waves. Then, the vectors determined by $\sin(k\theta_j \cdot X)$ and $\cos(k\theta_j \cdot X)$ are chosen, on each edge of Υ', as columns of Q_b in the FETI-DP algorithm for solving Helmholtz problems.

For problems that involve elastic solids (4) the plane waves are, cf. [11],

$$\begin{aligned}
v \ &= \ \sum_{j=1}^{n_w} \left\{ a_{p_j} \ \left(\beta_j \sin(k_p\theta_j \cdot X) + \gamma_j \cos(k_p\theta_j \cdot X)\right) \right\} \\
&+ \ \sum_{j=1}^{n_w} \left\{ a_{s_{1_j}} \left(\delta_j \sin(k_s\theta_j \cdot X) + \zeta_j \cos(k_s\theta_j \cdot X)\right) \right\} \\
&+ \ \sum_{j=1}^{n_w} \left\{ a_{s_{2_j}} \left(\eta_j \sin(k_s\theta_j \cdot X) + \xi_j \cos(k_s\theta_j \cdot X)\right) \right\},
\end{aligned} \tag{23}$$

where $a_{p_j} \in \mathbb{R}^3$ is a vector that is parallel to θ_j, $(a_{s_{1_j}}, a_{s_{2_j}}) \in \mathbb{R}^3 \times \mathbb{R}^3$ are two independent vectors in the plane orthogonal to θ_j,

$$k_p = \sqrt{\frac{\rho_e \omega^2}{\Lambda + 2\mu}}, \quad \text{and} \quad k_s = \sqrt{\frac{\rho_e \omega^2}{\mu}}, \tag{24}$$

are the pressure (longitudinal) and shear (transversal) wavenumbers, β_j, γ_j, δ_j, ζ_j, η_j, and ξ_j are real coefficients. Then the columns of Q_b can be chosen to represent the basis functions

in (23), on each edge of Υ'. Plane waves for the shell structures and their applications in FETI-DP can be found in [12].

The above extension of the FETI-DP algorithm to indefinite problems based on using Q_b with columns representing the plane waves is called FETI-DPH. It has been successful for solving both the elastic vibration problems and the acoustic problems, cf. [11, 12, 6]; for a fixed frequency, the FETI-DPH method is numerically scalable with respect to the number of subdomains and the problem size. The convergence analysis of a variant of the FETI-DPH algorithm for the Helmholtz equations can be found in [18].

4. Extension of FETI-DPH to fluid-structure interaction problems

Extensions of FETI-H and FETI-DP to FSI problems have been studied by Mandel [19], Walsh *et. al.* [23], and Dey and Datta [5]. However, the performance of these previous extensions in three dimensions is far from satisfactory. The alternative approach proposed in this paper recognizes that it is important to include some degrees of freedom on the fluid-structure interface in the coarse problem. The simpler case of a single mesh (conforming on the fluid-structure interface) for both the fluid and the structure region is discussed first. Then, it is generalized to the case of in-general non-matching, separate fluid and structure meshes.

4.1. Case of a single fluid-structure mesh

In this case, the fluid and structure meshes coincide on the fluid-structure interface Γ, which is formed by the common fluid-structure element faces. This single mesh is decomposed into subdomains. A typical decomposition of the domain is shown in Figure 2 for a two-dimensional example, where the fluid is on the left and the structure is on the right, separated by the interface Γ, represented by the dotted line in the figure. In this decomposition, subdomains Ω_4 and Ω_5 are pure fluid and structure subdomains, respectively. Ω_3 contains both fluid and structure elements and includes a part of the fluid-structure interface within it. Subdomains Ω_1 and Ω_2 are in the fluid region and the structure region, respectively, and they match on Γ_w, the subdomain fluid-structure interface boundary. The same type of subdomains also appears in the decomposition of three-dimensional meshes.

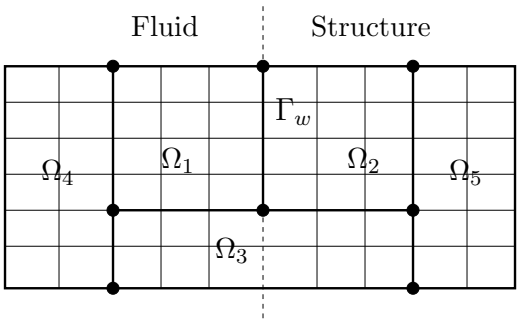

Figure 2. Decomposition of a combined fluid-structure domain.

Given the subdomain meshes, to define the FETI-DPH algorithm, the main step is to specify the coarse level degrees of freedom in the system (17). Following the standard selection of corner nodes, the dark black nodes in the decomposition shown in Figure 2 are chosen as subdomain corners and the corresponding degrees of freedom become coarse level degrees of freedom shared by the neighboring subdomains. With the coarse level degrees of freedom selected in (17), Lagrange multipliers are introduced to enforce the continuity for the other subdomain boundary degrees of freedom. For the example shown in Figure 2, Lagrange multipliers are introduced to enforce the continuity of fluid pressures across the subdomain boundaries shared by Ω_1 and Ω_4, by Ω_1 and Ω_3, and by Ω_3 and Ω_4, and the continuity of structural displacements shared by Ω_2 and Ω_5, Ω_2 and Ω_3, and by Ω_3 and Ω_5. In addition, the optional plane wave continuity constraints determined by (22) and by (23) can also be added on the subdomain boundaries to accelerate the convergence. The degrees of freedom on the fluid-structure interface within subdomain Ω_3 are simply treated as subdomain interior degrees of freedom.

The main difficulty of extending the FETI-DPH algorithm to FSI problems consists in handling degrees of freedom on the subdomain fluid-structure interface boundary Γ_w. Let the pressure and structural degrees of freedom on nodes of Γ_w be represented by p_w and $\mathbf{u}_w$, respectively. Denote C_w the matrix representing the FSI $\int_{\Gamma_w} p_w \mathbf{u}_w \cdot \mathbf{n}$, with appropriate scaling as in (9). There are the following three approaches for handling the FSI to generate subdomain problem matrices for Ω_1 and Ω_2.

(I) Artificial fluid degrees of freedom, represented by $p_w^{(2)}$, are introduced on Γ_w for the structure subdomain Ω_2; see Figure 3.

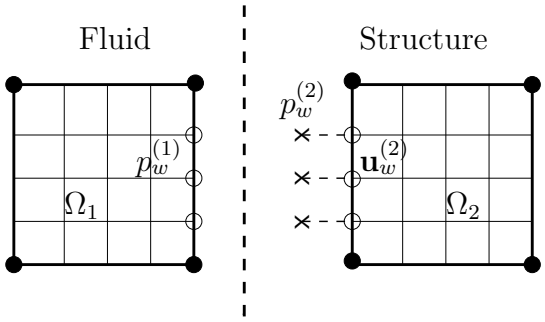

Figure 3. Fluid-structure interaction assigned to the structure subdomain.

The FSI is assigned to Ω_2 only and the subdomain problem matrices for Ω_1 and Ω_2 are

$$\begin{bmatrix} A_{rr}^{f(1)} & A_{rc}^{f(1)} & A_{rw}^{f(1)} \\ A_{cr}^{f(1)} & A_{cc}^{f(1)} & A_{cw}^{f(1)} \\ A_{wr}^{f(1)} & A_{wc}^{f(1)} & A_{ww}^{f(1)} \end{bmatrix}, \quad \text{and} \quad \begin{bmatrix} A_{rr}^{e(2)} & A_{rc}^{e(2)} & A_{rw}^{e(2)} & 0 \\ A_{cr}^{e(2)} & A_{cc}^{e(2)} & A_{cw}^{e(2)} & 0 \\ A_{wr}^{e(2)} & A_{wc}^{e(2)} & A_{ww}^{e(2)} & C_w^T \\ 0 & 0 & C_w & 0 \end{bmatrix},$$

where the superscripts f and e denote the fluid and structure blocks, respectively. The subscript w indicates blocks related to the subdomain fluid-structure interface degrees of freedom on Γ_w.

(II) Artificial structure degrees of freedom, represented by $\mathbf{u}_w^{(1)}$, are introduced on Γ_w for the fluid subdomain Ω_1; see Figure 4.

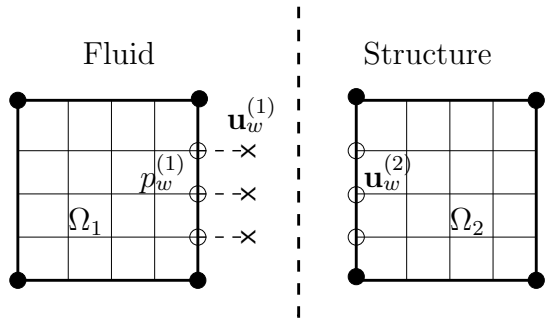

Figure 4. Fluid-structure interaction assigned to the fluid subdomain.

The FSI is assigned to Ω_1 only and the subdomain problem matrices for Ω_1 and Ω_2 are

$$\begin{bmatrix} A_{rr}^{f(1)} & A_{rc}^{f(1)} & A_{rw}^{f(1)} & 0 \\ A_{cr}^{f(1)} & A_{cc}^{f(1)} & A_{cw}^{f(1)} & 0 \\ A_{wr}^{f(1)} & A_{wc}^{f(1)} & A_{ww}^{f(1)} & C_w \\ 0 & 0 & C_w^T & 0 \end{bmatrix}, \quad \text{and} \quad \begin{bmatrix} A_{rr}^{e(2)} & A_{rc}^{e(2)} & A_{rw}^{e(2)} \\ A_{cr}^{e(2)} & A_{cc}^{e(2)} & A_{cw}^{e(1)} \\ A_{wr}^{e(1)} & A_{wc}^{e(2)} & A_{ww}^{e(2)} \end{bmatrix}.$$

(III) Artificial degrees of freedom, $\mathbf{u}_w^{(1)}$ and $p_w^{(2)}$, are introduced on Γ_w for both the fluid and the structure subdomains, respectively; see Figure 5.

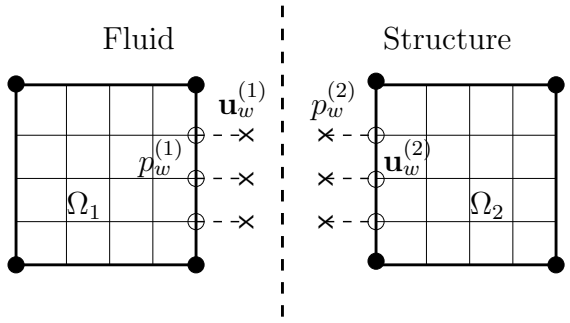

Figure 5. Fluid-structure interaction assigned to both structure and fluid subdomains.

The FSI is evenly distributed to Ω_1 and Ω_2, and the subdomain matrices are

$$\begin{bmatrix} A_{rr}^{f(1)} & A_{rc}^{f(1)} & A_{rw}^{f(1)} & 0 \\ A_{cr}^{f(1)} & A_{cc}^{f(1)} & A_{cw}^{f(1)} & 0 \\ A_{wr}^{f(1)} & A_{wc}^{f(1)} & A_{ww}^{f(1)} & \frac{1}{2}C_w \\ 0 & 0 & \frac{1}{2}C_w^T & 0 \end{bmatrix}, \quad \text{and} \quad \begin{bmatrix} A_{rr}^{e(2)} & A_{rc}^{e(2)} & A_{rw}^{e(2)} & 0 \\ A_{cr}^{e(2)} & A_{cc}^{e(2)} & A_{cw}^{e(2)} & 0 \\ A_{wr}^{e(2)} & A_{wc}^{e(2)} & A_{ww}^{e(2)} & \frac{1}{2}C_w^T \\ 0 & 0 & \frac{1}{2}C_w & 0 \end{bmatrix}.$$

These three approaches have been discussed by Walsh *et al* [23] in the time domain context. In their work, the first approach was chosen; the other two approaches can lead to singular fluid subdomain problem matrices. The modification of the FETI-DPH algorithm proposed in this paper also follows the first approach and assigns all FSI to subdomains containing the structural elements connected to the fluid-structure interface. Another advantage of the first approach compared with the other two is that fewer artificial degrees of freedom are introduced on the subdomain fluid-structure interface boundary Γ_w. Since for each node there is only one pressure degree of freedom, but there are at least three structure degrees of freedom, fewer Lagrange multipliers need to be used in the FETI-DPH algorithm to enforce the continuity of those variables across Γ_w.

In the previous extensions of the FETI-DP algorithm to FSI problems [23, 5], the coarse problem contains only the standard subdomain corners selected in the original FETI-DP algorithm. However the standard selection is not sufficient for FSI problems and as a result, the convergence rate of such extensions is very poor, especially for large three-dimensional problems. Here, three choices of the coarse level degrees of freedom for the FSI problems are discussed. The numerical experiments in Section 5 show that, to obtain satisfactory performance of the FETI-DPH algorithm for FSI problems, an appropriate choice of the coarse level variables on the subdomain fluid-structure interface boundary is crucial.

The system of equations (17) for FSI problems can be written in the following detailed form

$$\begin{bmatrix} A_{rr} & A^e_{rw} & A^f_{rw} & \widetilde{A}_{rc} & B_r^T \\ A^e_{wr} & A^e_{ww} & C_w^T & \widetilde{A}^e_{wc} & B_w^{e^T} \\ A^f_{wr} & C_w & A^f_{ww} & \widetilde{A}^f_{wc} & B_w^{f^T} \\ \widetilde{A}_{cr} & \widetilde{A}^e_{cw} & \widetilde{A}^f_{cw} & \widetilde{A}_{cc} & 0 \\ B_r & B^e_w & B^f_w & 0 & 0 \end{bmatrix} \begin{bmatrix} \mathbf{u}p_r \\ \mathbf{u}_w \\ p_w \\ \widetilde{\mathbf{u}p}_c \\ \lambda \end{bmatrix} = \begin{bmatrix} b_r \\ b^e_w \\ b^f_w \\ \widetilde{b}_c \\ 0 \end{bmatrix}, \tag{25}$$

where A_{rr} is block diagonal with each block corresponding to one subdomain. Each subdomain can be either a fluid subdomain, a structure subdomain, or a mixed subdomain containing both fluid and structure elements as illustrated in Figure 2. The notation $\mathbf{u}p_r$ is used to represent independent subdomain degrees of freedom. The vectors $\mathbf{u}_w$ and p_w represent the structure and fluid degrees of freedom on the subdomain fluid-structure interface boundary, respectively. They can either be chosen as coarse level degrees of freedom or as independent subdomain degrees of freedom, which will lead to different cases of the algorithm as discussed below. If $\mathbf{u}_w$ and p_w are chosen as independent subdomain variables, Lagrange multipliers need to be introduced through the Boolean matrices B^e_w and B^f_w to enforce their continuity across the subdomain boundaries. The vector $\widetilde{\mathbf{u}p}_c$ represents the standard corner degrees of freedom selected in the FETI-DP algorithm and the set of Lagrange multipliers enforcing the optional continuity constraints corresponding to the plane waves for indefinite problems.

Writing (25) in the compact form of (17) by specifying the groups of subdomain independent variables x_r and the coarse level variables $\widetilde{x}_c$, the FETI-DPH algorithm then follows directly as presented for (17)–(19).

4.1.1. Algorithm C1 - no additional coarse degrees of freedom on the subdomain fluid-structure interface boundary This approach is a straightforward application of FETI-DPH to the FSI problems, using the standard selection of corner nodes in the FETI-DPH method. It was used

by Dey and Datta [5] and Walsh *et al.* [23] in their application of FETI-DP to FSI problems. The coarse level variables are only $\widetilde{\mathbf{u}p}_c$. The subdomain fluid-structure interface boundary variables $\mathbf{u}_w$ and p_w are all independent subdomain variables and Lagrange multipliers are used to enforce their continuity across subdomain boundaries. The blocks of (25) can be grouped as

$$\begin{bmatrix} \boxed{\begin{matrix} A_{rr} & A^e_{rw} & A^f_{rw} \\ A^e_{wr} & A^e_{ww} & C^T_w \\ A^f_{wr} & C_w & A^f_{ww} \end{matrix}} & \begin{matrix} \widetilde{A}_{rc} \\ \widetilde{A}^e_{wc} \\ \widetilde{A}^f_{wc} \end{matrix} & \begin{matrix} B_r^T \\ B_w^{e\,T} \\ B_w^{f\,T} \end{matrix} \\ \begin{matrix} \widetilde{A}_{cr} & \widetilde{A}^e_{cw} & \widetilde{A}^f_{cw} \end{matrix} & \widetilde{A}_{cc} & 0 \\ \begin{matrix} B_r & B^e_w & B^f_w \end{matrix} & 0 & 0 \end{bmatrix} \begin{bmatrix} \boxed{\begin{matrix} \mathbf{u}p_r \\ \mathbf{u}_w \\ p_w \end{matrix}} \\ \widetilde{\mathbf{u}p}_c \\ \lambda \end{bmatrix} = \begin{bmatrix} \boxed{\begin{matrix} b_r \\ b^e_w \\ b^f_w \end{matrix}} \\ \widetilde{b}_c \\ 0 \end{bmatrix}.$$

The compact form of (17) can be obtained with the following choices

$$x_r := \begin{bmatrix} \mathbf{u}p_r \\ \mathbf{u}_w \\ p_w \end{bmatrix}, \quad \widetilde{x}_c := \widetilde{\mathbf{u}p}_c, \quad A_{rr} := \begin{bmatrix} A_{rr} & A^e_{rw} & A^f_{rw} \\ A^e_{wr} & A^e_{ww} & C^T_w \\ A^f_{wr} & C_w & A^f_{ww} \end{bmatrix}, \quad \widetilde{A}_{cc} := \widetilde{A}_{cc}, \quad \text{etc.}$$

Then, the FETI-DPH algorithm for the FSI problem consists in iterating on the interface problem (18).

4.1.2. Algorithm C2 - fluid degrees of freedom on the subdomain fluid-structure interface boundary in the coarse problem The fluid degrees of freedom p_w, together with $\widetilde{\mathbf{u}p}_c$, are used as the coarse level degrees of freedom in the FETI-DPH algorithm. The structure degrees of freedom $\mathbf{u}_w$ on the subdomain fluid-structure interface boundary are independent subdomain variables. The blocks of (25) can be grouped as follows

$$\begin{bmatrix} \boxed{\begin{matrix} A_{rr} & A^e_{rw} \\ A^e_{wr} & A^e_{ww} \end{matrix}} & \begin{matrix} A^f_{rw} & \widetilde{A}_{rc} \\ C^T_w & \widetilde{A}^e_{wc} \end{matrix} & \begin{matrix} B_r^T \\ B_w^{e\,T} \end{matrix} \\ \begin{matrix} A^f_{wr} & C_w \\ \widetilde{A}_{cr} & \widetilde{A}^e_{cw} \end{matrix} & \boxed{\begin{matrix} A^f_{ww} & \widetilde{A}^f_{wc} \\ \widetilde{A}^f_{cw} & \widetilde{A}_{cc} \end{matrix}} & \begin{matrix} 0 \\ 0 \end{matrix} \\ \begin{matrix} B_r & B^e_w \end{matrix} & \begin{matrix} 0 & 0 \end{matrix} & 0 \end{bmatrix} \begin{bmatrix} \boxed{\begin{matrix} \mathbf{u}p_r \\ \mathbf{u}_w \end{matrix}} \\ \boxed{\begin{matrix} p_w \\ \widetilde{\mathbf{u}p}_c \end{matrix}} \\ \lambda \end{bmatrix} = \begin{bmatrix} \boxed{\begin{matrix} b_r \\ b^e_w \end{matrix}} \\ \boxed{\begin{matrix} b^f_w \\ \widetilde{b}_c \end{matrix}} \\ 0 \end{bmatrix}.$$

The compact form of (17) is then obtained with the following choices

$$x_r := \begin{bmatrix} \mathbf{u}p_r \\ \mathbf{u}_w \end{bmatrix}, \quad \widetilde{x}_c := \begin{bmatrix} p_w \\ \widetilde{\mathbf{u}p}_c \end{bmatrix}, \quad A_{rr} := \begin{bmatrix} A_{rr} & A^e_{rw} \\ A^e_{wr} & A^e_{ww} \end{bmatrix}, \quad \widetilde{A}_{cc} := \begin{bmatrix} A^f_{ww} & \widetilde{A}^f_{wc} \\ \widetilde{A}^f_{cw} & \widetilde{A}_{cc} \end{bmatrix}, \quad \text{etc.}$$

Then, the FETI-DPH algorithm follows again from (18) with the choices made above.

4.1.3. Algorithm C3 - all subdomain fluid-structure interface boundary variables in the coarse problem In this approach, all $\mathbf{u}_w$ and p_w are chosen as coarse level degrees of freedom, together

with $\widetilde{\mathbf{u}p}_c$. Correspondingly, the blocks of (25) are grouped as follows

$$\begin{bmatrix} A_{rr} & A^e_{rw} & A^f_{rw} & \widetilde{A}_{rc} & B^T_r \\ A^e_{wr} & A^e_{ww} & C^T_w & \widetilde{A}^e_{wc} & 0 \\ A^f_{wr} & C_w & A^f_{ww} & \widetilde{A}^f_{wc} & 0 \\ \widetilde{A}_{cr} & \widetilde{A}^e_{cw} & \widetilde{A}^f_{cw} & \widetilde{A}_{cc} & 0 \\ B_r & 0 & 0 & 0 & 0 \end{bmatrix} \begin{bmatrix} \mathbf{u}p_r \\ \mathbf{u}_w \\ p_w \\ \widetilde{\mathbf{u}p}_c \\ \lambda \end{bmatrix} = \begin{bmatrix} b_r \\ b^e_w \\ b^f_w \\ \widetilde{b}_c \\ 0 \end{bmatrix}.$$

The compact form of (17) is then obtained with

$$x_r := \mathbf{u}p_r, \quad \widetilde{x}_c := \begin{bmatrix} \mathbf{u}_w \\ p_w \\ \widetilde{\mathbf{u}p}_c \end{bmatrix}, \quad A_{rr} := A_{rr}, \quad \widetilde{A}_{cc} := \begin{bmatrix} A^e_{ww} & C^T_w & \widetilde{A}^e_{wc} \\ C_w & A^f_{ww} & \widetilde{A}^f_{wc} \\ \widetilde{A}^e_{cw} & \widetilde{A}^f_{cw} & \widetilde{A}_{cc} \end{bmatrix}, \quad \text{etc.}$$

At each subdomain fluid-structure interface boundary node, there is only one pressure degree of freedom, compared with three structural displacements, and another three rotations for fourth-order problems. Choosing only the pressure degrees of freedom p_w as coarse level variables thus generates a much smaller coarse problem than choosing both p_w and $\mathbf{u}_w$ as coarse level variables. The numerical experiments in Section 5 indicate that including only p_w in the coarse level problem (Algorithm C2) improves the convergence rate, as well as the CPU time, compared with using the original FETI-DPH method (Algorithm C1). Including both p_w and $\mathbf{u}_w$ in the coarse problem (Algorithm C3) can further reduce the iteration count, but the CPU time trade-off is problem dependent due to increased coarse space sizes.

4.2. Case of separate fluid and structure meshes

In many practical applications, separate meshes for the fluid and the structure are used, i.e., the fluid and structure meshes have their own sets of nodes, and at the fluid-structure interface the fluid nodes and the structure nodes are in general not matching; see Figure 6 for a typical illustration of a two-dimensional case with *overlaps* and *gaps* between the fluid and structure meshes. Several complications arise in extending FETI-DPH for this type of problems as discussed below.

4.2.1. Fluid-structure interaction matrix for separate meshes The basic idea used in this paper to form the FSI block C_Γ in (8) corresponding to

$$\int_\Gamma p\mathbf{v}\cdot\mathbf{n}$$

follows the approach of *Algorithms for Contact in a Multiphysics Environment* (ACME) [4] developed by the Sandia National Laboratories. Some other approaches and their comparison can be found in [3] and the references therein. In the case of separate fluid and structure meshes, the fluid-structure interface Γ needs first to be defined. In general, the fluid-structure interface defined by the fluid mesh is different from that defined by the structure mesh. Let Γ_f represent the faces of the fluid elements on the fluid-structure boundary and Γ_e the faces of the structure elements. Either Γ_f or Γ_e can be taken as the fluid-structure interface Γ; here

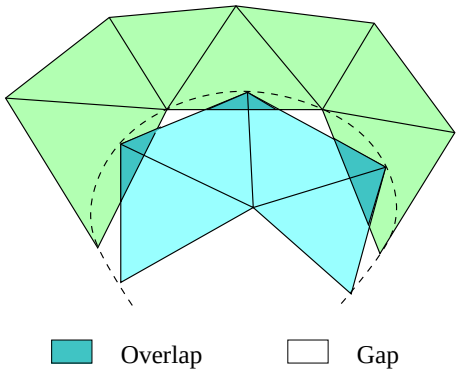

Figure 6. Separate fluid and structure meshes with overlaps and gaps (two-dimensional case).

Γ_f is adopted as Γ because in practical applications the fluid mesh is often finer than the structural mesh. A minimal distance projection is used to provide an association between the two meshes as described below.

Let $\phi_j^f(x)$ represent a finite element basis function defined on a face $\gamma_f \subset \Gamma_f$ and let $\psi_k^e(x)$ be a finite element function defined on $\gamma_e \subset \Gamma_e$. The face γ_e is projected onto Γ_f by a minimal distance projection and the part projected onto γ_f is denoted by $\gamma_{f\cap e}$, as illustrated in Figure 7.

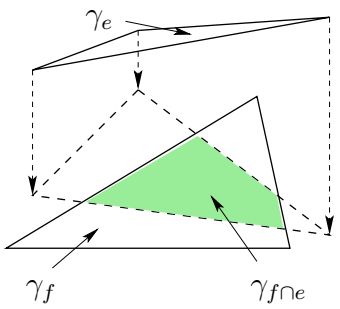

Figure 7. Projection of a structure element face γ_e onto a fluid element face γ_f.

Then, C_Γ is assembled from contributions of the type

$$\int_{\gamma_{f\cap e}} \phi_j^f(x)\ \psi_k^e(Mx)\ dx, \tag{26}$$

where M represents the map from $\gamma_{f\cap e}$ to γ_e.

4.2.2. Decomposition of separate fluid and structure meshes Without a nodal connection of the fluid and structure meshes, a nodal topology based decomposer will generate subdomains which contain either fluid elements or structure elements only. As a result, all nodes on the fluid-structure interface become subdomain boundary nodes, leading to a large coarse problem

in the FETI-DPH Algorithms C2 and C3 discussed in Sections 4.1.2 and 4.1.3. It is therefore preferable that more of the FSI be included within subdomains, in which case fewer degrees of freedom on the fluid-structure interface appear on the subdomain boundaries, and the FSI within the subdomains can be handled well by solving subdomain problems directly.

The algorithm proposed here to decompose the separate fluid and structural meshes into subdomains aims to create subdomains surrounding the fluid-structure interface that are as thin as possible, but thick enough to include the interface inside. In this way, the fluid-structure interface will be enclosed in a union of pancake shaped subdomains, allowing more of the FSI to be included in the interior of subdomains.

For each pair p_w, a fluid degree of freedom, and $\mathbf{u}_w$, a structure degree of freedom, such that the corresponding entry in C_Γ is non-zero, a FSI element is introduced to connect the separate fluid and structure meshes together. Given all the fluid, structure, and FSI elements, and the number of subdomains, the decomposer determines the `average_load` for the subdomains. Then, it starts from an arbitrary FSI element, labeled the `current_element`, and assigns it to the first subdomain, labeled the `current_subdomain`. The decomposer then assigns all yet unassigned elements connected with `current_element` to either the `higher_priority_queue` or the `lower_priority_queue`, depending on whether a node of that element is on the fluid-structure interface or not. A new `current_element` is then taken from the front of `higher_priority_queue` if it is not empty, otherwise from the front of `lower_priority_queue`, and is assigned either to `current_subdomain` or to a new `current_subdomain`, depending on whether the `current_subdomain` is overloaded or not. An outline of this algorithm is presented in Algorithm 1.

Algorithm 1 Decomposition of separate fluid and structure meshes into subdomains.

1: Given the number of subdomains and set of elements, determine `average_load` of the subdomains and set $j = 1$.
2: Start from one FSI element, name it the `current_element`, and assign it to Ω_j, the `current_subdomain`.
3: **repeat**
4: Do for all unassigned elements connected to `current_element`: if they have a node on the fluid-structure interface, assign them to `high_priority_queue`, otherwise to `low_priority_queue`.
5: If `high_priority_queue` is not empty, take its front element as `current_element`, otherwise take the front of `low_priority_queue` as `current_element`.
6: If the number of degrees of freedom in `current_subdomain` is less than `average_load`, assign `current_element` to `current_subdomain`, otherwise assign it to a new subdomain – the new `current_subdomain`. Increase j by 1.
7: **until** `high_priority_queue` and `low_priority_queue` are both empty.

4.2.3. Extension of the FETI-DPH algorithm to problems with separate fluid and structure meshes The same formulation as that discussed in Section 4.1 for the single mesh case is also valid for the case of separate meshes. One can choose either the standard coarse level variables selected in FETI-DPH (Algorithm C1), or include the fluid degrees of freedom on the subdomain fluid-structure interface boundary in the coarse problem (Algorithm C2), or

include both the fluid and the structural degrees of freedom on the subdomain fluid-structure interface boundary in the coarse problem (Algorithm C3).

5. Numerical experiments

The proposed extension of the FETI-DPH algorithm is applied to the solution of several FSI problems. A GMRES iteration with Dirichlet preconditioner is implemented to solve the dual problem (18). The iteration is stopped when the residual of the original problem (9) is reduced by 10^{-6}. All the experiments are run in parallel on 32 cores of a Linux cluster, except those reported in Table IV which are performed on up to 128 cores to study the parallel scalability of the proposed algorithm. In particular, the coarse problems in the algorithm are solved in parallel by using the multifrontal massively parallel sparse direct solver (MUMPS), cf. [1].

In all the tables of this section, k represents the fluid wavenumber in (3), #sub represents the number of subdomains, #aug represents the number of directions of the plane waves added in the coarse problem, "wet corner" represents the three different choices of the coarse level variables on the subdomain fluid-structure interface boundary in the FETI-DPH algorithm as discussed in Section 4: Algorithm C1 with no additional coarse level variables selected on the subdomain fluid-structure interface boundary; Algorithm C2 when selecting all the pressure degrees of freedom; and Algorithm C3 with both the pressure and the structural degrees of freedom. Besides the iteration count and total CPU time, the size of the coarse problem and the CPU time for forming and solving coarse problems are also reported.

5.1. A solid cube immersed in a spherical fluid domain

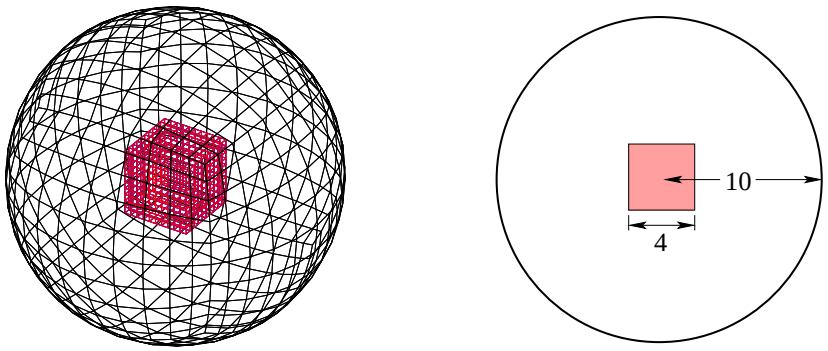

Figure 8. A solid cube immersed in a spherical fluid domain.

In the first set of experiments, the scattering of a planar time-harmonic acoustic wave by an elastic solid cube made of steel and immersed in a spherical fluid (water) domain is considered; see Figure 8. The dimensions of the solid cube are $4 \times 4 \times 4$ and the radius of the fluid sphere is 10. A single mesh of trilinear hexahedral elements (8 nodes per element) is used to discretize

the fluid and solid domains. Three different mesh sizes, $32 \times 32 \times 32$, $40 \times 40 \times 40$, and $50 \times 50 \times 50$, are used to discretize the solid cube. The solid mesh is extended from each face of the cube into the fluid domain by 32, 40 and 50 layers of fluid elements, respectively, which gives $6 \times 32 \times 32 \times 32$, $6 \times 40 \times 40 \times 40$, $6 \times 50 \times 50 \times 50$ elements in the fluid region. This results in 310,629, 600,445, and 1,163,055 degrees of freedom, respectively. Two fluid wavenumbers are considered, namely, $k = 2$ and $k = 4$.

Tables I and II show the dependence of the iteration count and CPU time of the proposed FETI-DPH algorithm on the number of subdomains, and on the choices of the coarse level variables on the subdomain fluid-structure interface boundary for the smallest and the largest mesh. For a problem of a given size, the iteration count decreases with the number of subdomains, and with including more degrees of freedom on the subdomain fluid-structure interface boundary as coarse level variables. The fastest convergence from the CPU viewpoint is achieved when only the pressure degrees of freedom on the subdomain fluid-structure interface boundary are included in the coarse problem (Algorithm C2). Including both the pressure and the displacement variables in the coarse problem (Algorithm C3) results in lower iteration counts, but does not improve the overall CPU time, because this generates larger coarse problems to solve. Without using any additional coarse degrees of freedom on the subdomain fluid-structure interface boundary, the convergence is very slow both in iteration count and in CPU time. The tables also indicate that solving the coarse problems consumes the major part of the total CPU time when the additional coarse degrees of freedom are employed.

Table I. Solid cube in fluid sphere, 310,629 dof, $k = 2$ and $k = 4$.

k	#sub	#aug	wet corner	coarse size	iteration count	total CPU time (s)	coarse CPU time
2	64	3	C1	4,538	340	51.1	16.3
			C2	6,285	34	21.3	17.0
			C3	11,593	31	37.4	33.2
	128	3	C1	8,208	293	40.2	15.7
			C2	10,102	25	13.4	10.9
			C3	15,807	21	23.0	20.8
	256	3	C1	15,332	253	36.8	28.6
			C2	17,852	19	**10.6**	9.0
			C3	24,732	16	15.5	14.1
4	64	5	C1	6,433	1,374	257.9	61.1
			C2	8,279	144	42.7	28.4
			C3	13,506	139	61.1	46.6
	128	5	C1	11,615	1,407	267.7	72.6
			C2	13,651	140	34.6	23.7
			C3	19,216	137	46.4	35.4
	256	5	C1	21,226	1,223	271.2	113.8
			C2	24,061	102	**31.0**	24.2
			C3	30,772	101	40.3	33.5

Tables III and IV demonstrate the parallel scalability of the proposed FETI-DPH algorithm. When the size of the problem is doubled while keeping the size of the subdomain problems

Table II. Solid cube in fluid sphere, 1,163,055 dof, $k = 2$ and $k = 4$.

k	#sub	#aug	wet corner	coarse size	iteration count	total CPU time (s)	coarse CPU time
2	256	3	C1	17,398	300	154.7	54.2
			C2	20,987	26	67.2	54.2
			C3	32,177	18	105.2	94.9
	512	3	C1	32,201	293	140.4	61.9
			C2	36,728	20	**48.2**	40.8
			C3	50,589	15	77.7	71.3
	1,024	3	C1	58,505	301	163.0	88.1
			C2	63,980	18	52.5	46.5
			C3	80,238	15	79.5	74.5
4	256	5	C1	24,585	1,237	715.6	170.8
			C2	28,457	93	116.9	83.9
			C3	39,461	86	161.6	129.8
	512	5	C1	44,966	929	535.6	199.1
			C2	50,004	60	98.7	77.6
			C3	63,524	56	123.5	106.7
	1,024	5	C1	80,176	661	479.7	247.9
			C2	86,439	32	**98.1**	91.7
			C3	102,180	29	145.9	137.5

Table III. Scalability with respect to the problem size.

k	#aug	number of dof	#sub	iteration count	total CPU time on 32 cores
2	3	310,629	256	19	10.6
		600,445	512	19	22.2
		1,163,055	1,024	18	52.5
	5	310,629	256	18	13.1
		600,445	512	18	27.2
		1,163,055	1,024	17	63.0
4	3	310,629	256	180	33.7
		600,445	512	120	65.0
		1,163,055	1,024	57	82.7
	5	310,629	256	102	31.0
		600,445	512	62	46.4
		1,163,055	1,024	32	98.1

similar, the iteration count does not increase and the CPU time is approximately doubled as shown in Table III. Table IV reports the CPU performance associated with solving the largest problem with 1,163,055 dof on up to 128 CPU cores. The speed-up is around 1.85 when the number of cores is increased from 2 to 4, 5.70 when the number of cores is increased from 2 to 16, and around 20 when increased from 2 to 128. Therefore, the parallel scalability of the overall FETI-DPH algorithm is limited for this setup by that of the coarse problem solver.

Table IV. Parallel scalability (solid cube in a fluid sphere — 1,163,055 dof.

	number of	FETI-DPH solver total		coarse problem part		
k	CPU cores	CPU time	speed-up	CPU time	(% in total CPU)	speed-up
2	2	491.7	1	380.1	(77.3%)	1
	4	269.0	1.83	212.0	(78.8%)	1.79
	8	160.7	3.06	131.5	(81.8%)	2.89
	16	84.8	5.80	69.9	(82.4%)	5.43
	32	48.2	10.20	40.8	(84.6%)	9.31
	64	29.1	16.90	25.3	(86.9%)	15.02
	128	23.4	21.01	20.8	(88.9%)	18.27
4	2	782.2	1	584.8	(74.8%)	1
	4	417.5	1.87	316.4	(75.8%)	1.85
	8	231.7	3.36	181.1	(78.2%)	3.23
	16	139.7	5.60	113.7	(81.4%)	5.15
	32	82.7	9.46	68.4	(82.7%)	8.56
	64	50.9	15.37	43.7	(85.9%)	13.41
	128	40.2	19.46	34.9	(86.8%)	16.79

5.2. Mockup submarine problem

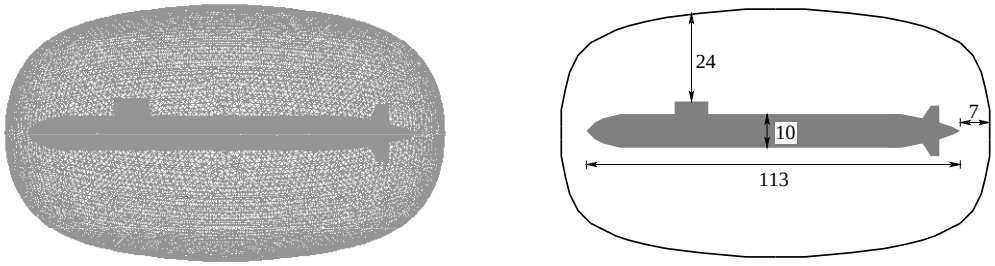

Figure 9. A submarine model immersed in a fluid.

Next, planar wave scattering from a submerged mockup submarine (see Figure 9) is considered with $k = 0.5$. The scatterer is modeled as an elastic shell structure of length $l = 113$. Linear tetrahedral elements are used to discretize the fluid region. The projection of the fluid mesh onto the submarine surface provides a triangular discretization with three-noded shell elements for the mockup submarine. To this effect, two fluid meshes are considered: one with 309,535 dof, and one with 691,816 degrees of freedom. These contain about 226 and 520 elements along the length of the mockup submarine, respectively.

The performance of FETI-DPH obtained for this problem is given in Table V. For a fixed problem size, the iteration count decreases with the number of subdomains and with the

Table V. Performance of FETI-DPH for the mockup submarine problem with $k = 0.5$.

number of dof	#sub	#aug	wet corner	coarse size	iteration count	total CPU time
309,535	64	5	C2	8,138	299	62.3
			C3	19,982	51	72.4
		7	C2	10,034	210	50.3
			C3	21,044	35	79.2
	128	5	C2	13,302	195	36.7
			C3	26,490	32	40.1
		7	C2	16,395	140	39.7
			C3	28,464	21	40.1
	256	5	C2	22,194	135	31.0
			C3	37,500	14	**25.8**
		7	C2	26,708	121	35.4
			C3	40,742	11	30.7
691,816	128	5	C2	13,415	125	57.6
			C3	26,798	14	82.2
		7	C2	16,497	98	60.7
			C3	28,902	11	86.9
	256	5	C2	22,704	166	55.9
			C3	37,449	13	49.8
		7	C2	27,743	147	65.3
			C3	41,315	10	51.3
	512	5	C2	38,605	135	50.8
			C3	55,996	12	**42.3**
		7	C2	46,284	123	62.3
			C3	62,439	11	46.1

number of plane waves used in the augmentation. Doubling the problem size roughly doubles the CPU time, provided that the subdomain size is kept similar. Including both the pressure and structural degrees of freedom on the subdomain fluid-structure interface boundary in the coarse problem (Algorithm C3) gives a much more substantial reduction in the iteration count, compared with the example discussed in Section 5.1. The best CPU time is achieved with this choice on 32 cores. If significantly more cores are used, the algorithm including only the pressure degrees of freedom in the coarse problem (Algorithm C2) prevails due to its smaller coarse problem size and associated parallel scalability. It is noted that the algorithm without the additional coarse space variables (Algorithm C1) fails to converge.

5.3. Coupled submarine models using separate fluid and structure meshes

The same problem as in Section 5.2 is solved here using however separate fluid and structure meshes. In particular, two different cases are considered. In the first case, the separate fluid and structure meshes are obtained by cutting the single mesh of 309,535 dof of Section 5.2 along the fluid-structure interface. In this case, the fluid and structure meshes have their own sets of nodes which match on the fluid-structure interface. In the second case, genuinely separate

Table VI. Performance of FETI-DPH for the mockup submarine problem, separate fluid and structure meshes, and $k = 0.5$.

number of dof	#sub	#aug	wet corner	coarse size	iteration count	total CPU time
Separate, but matching, fluid and structural meshes						
309,535	64	5	C2	6,920	504	69.1
			C3	15,104	201	69.1
		7	C2	8,477	340	58.0
			C3	16,151	131	61.7
	128	5	C2	11,690	273	36.7
			C3	21,794	104	40.4
		7	C2	14,381	167	31.9
			C3	23,669	64	35.2
	256	5	C2	20,312	217	34.6
			C3	34,214	44	26.0
		7	C2	24,566	161	36.8
			C3	37,274	30	**25.6**
Separate and non-matching fluid and structural meshes						
333,319	64	5	C2	12,273	599	172.7
			C3	22,113	228	161.1
		7	C2	13,995	447	158.6
			C3	23,343	173	151.8
	128	5	C2	17,716	461	143.1
			C3	30,808	115	134.5
		7	C2	20,658	322	121.2
			C3	32,907	86	136.8
	256	5	C2	29,515	369	105.5
			C3	47,506	77	**79.6**
		7	C2	34,339	269	100.5
			C3	50,926	60	87.2

non-matching fluid and structure meshes are generated to test the proposed solver.

The FSI elements are added into the element set and are used to decompose the meshes into subdomains as described in Section 4.2. The mesh decomposition Algorithm 1 allows more FSI to be included in the interior of subdomains. Comparing the top halves of Tables V and VI, one can observe that the new decomposer for the separate but matching fluid and structure meshes generates smaller coarse problems than using the standard decomposer for a single mesh. On the other hand, Table VI indicates that, if the fluid and structure meshes are genuinely separate and non-matching, larger coarse problems are obtained. This directly affects the CPU performance. Whereas the iteration count for both types of meshes are comparable, the CPU performance obtained for non-matching meshes reflects the larger size of the coarse problem.

6. Conclusions

In this paper, the FETI-DPH algorithm was extended to vibro-acoustic fluid-structure interaction FSI problems in the frequency domain. Several choices of the coarse level variables were discussed. It was shown that an appropriate selection of the coarse level primal degrees of freedom on the subdomain fluid-structure interface boundary is crucial for the fast convergence of the algorithm. Selecting only the standard coarse level variables as in the original FETI-DPH solver does not yield satisfactory results for the FSI problems. Including either the fluid degrees of freedom or both the fluid and structure degrees of freedom on the subdomain fluid-structure interface boundary in the coarse problem greatly improves the convergence rate of the FETI-DPH algorithm. The results of numerical experiments performed for realistic FSI problems demonstrated the numerical scalability of the proposed algorithm extension.

Acknowledgments

The authors acknowledge the support by the Office of Naval Research under Grant N00014-05-1-0204-1.

REFERENCES

1. P. R. Amestoy, I. S. Duff, J. Koster, and J.-Y. L'Excellent. A fully asynchronous multifrontal solver using distributed dynamic scheduling. *SIAM J. Matrix Anal. Appl.*, 23:15-41, 2001.
2. M. Bhardwaj, K. Pierson, G. Reese, T. Walsh, D. Day, C. Farhat, and M. Lesoinne. Salinas: a scalable software for high-performance structrual and solid mechanics simulations. *Proceedings of the IEEE/ACM SC2002 Conference*, Baltimore, Maryland, November 16-22, 2002.
3. A. de Boer, A. H. van Zuijlen, and H. Bijl. Review of coupling methods for non-matching meshes. *Comput. Methods Appl. Mech. Engrg,* 196:1515–1525, 2007.
4. K. H. Brown, M. W. Glass, A. S. Gullerud, M. W. Heinstein, R. E. Jones, and T. E. Voth. ACME: Algorithms for Contact in a Multiphysics Environment API Version 1.3. Technical Report SAND2003-1470, Sandia National Laboratories, Albuquerque, New Mexico, May 2003.
5. S. Dey and D. K. Datta. A parallel hp-FEM infrastructure for three-dimensional structural acoustics. *Internat. J. Numer. Methods Engrg.*, 68:583–603, 2006.
6. C. Farhat, P. Avery, R. Tezaur, and J. Li. A dual-primal domain decomposition method for acoustic scaterring. *J. of Comput. Acoustics*, 13:499–524, 2005.
7. C. Farhat, P. S. Chen, F. Risler, and F. X. Roux. A unified framework for accelerating the convergence of iterative substructuring methods with Lagrange multipliers. *Internat. J. Numer. Meths. Engrg.*, 42:257–288, 1998.
8. C. Farhat, M. Lesoinne, P. Le Tallec, K. Pierson, and D. Rixen. FETI-DP: A dual-primal unified FETI method – part I: A faster alternative to the two-level FETI method. *Internat. J. Numer. Methods Engrg.*, 50:1523–1544, 2001.
9. C. Farhat, M. Lesoinne, and K. Pierson. A scalable dual-primal domain decomposition method. *Numer. Linear Algebra Appl.*, 7:687–714, 2000.
10. C. Farhat, M. Lesoinne, P. LeTallec, K. Pierson, and D. Rixen. FETI-DP: a dual-primal unified FETI method - part I: a faster alternative to the two-level FETI method. *Internat. J. Numer. Meths. Engrg.*, 50:1523–1544, 2001.
11. C. Farhat and J. Li. An iterative domain decomposition method for the solution of a class of indefinite problems in computational structural dynamics. *Appl. Numer. Math.*, 54:150–166, 2005.
12. C. Farhat, J. Li, and P. Avery. A FETI–DP method for the parallel iterative solution of indefinite and complex-valued solid and shell vibration problems. *Internat. J. Numer. Methods Engrg.*, 63:398–427, 2005.
13. C. Farhat, A. Macedo, and M. Lesoinne. A two-level domain decomposition method for the iterative solution of high frequency exterior Helmholtz problems, *Numer. Math.*, 85:283–308, 2000.

14. C. Farhat and F.-X. Roux. A method of finite element tearing and interconnecting and its parallel solution algorithm. *Internat. J. Numer. Methods Engrg.*, 32:1205–1227, 1991.
15. A. Klawonn and O. B. Widlund. Dual-primal FETI methods for linear elasticity. *Comm. Pure Appl. Math.*, 59:1523–1572, 2006.
16. A. Klawonn, O. B. Widlund, and M. Dryja. Dual-primal FETI methods for three-dimensional elliptic problems with heterogeneous coefficients. *SIAM J. Numer. Anal.*, 40:159–179, 2002.
17. M. Lesoinne. A FETI-DP corner selection algorithm for three-dimensional problems. *Domain Decomposition Methods in Science and Engineering*, Proc. of the 14th international conference on domain decomposition methods, Natl. Auton. Univ. Mex., Mexico, 217–223, 2003.
18. J. Li and X. Tu. Convergence analysis of a balancing domain decomposition method for solving a class of indefinite linear systems. *Numer. Linear Algebra Appl.*, 16:745–773, 2009.
19. J. Mandel. An iterative substructuring method for coupled fluid-solid acoustic problems. *J. Comput. Phys.*, 177:95–116, 2002.
20. J. Mandel and R. Tezaur. On the convergence of a dual-primal substructuring method. *Numer. Math.*, 88:543–558, 2001.
21. H. Morand and R. Ohayon. *Fluid Structure Interaction*. John Wiley and Sons, Chichester, 1995.
22. R. Ohayon and C. Soize. *Structural Acoustics and Vibration*. Academic Press, London, 1998.
23. T. F. Walsh, G. M. Reese, K. H. Pierson, H. Sumali, J. L. Dohner, and D. M. Day. Computational and experimental techniques for coupled acoustic/structure interactions. Technical Report SAND2003-4381, Sandia National Laboratories, Albuquerque, New Mexico, January 2004.
24. A. Toselli and O. B. Widlund. *Domain Decomposition Methods - Algorithms and Theory*. Springer Verlag, Berlin-Heidelberg-New York, 2004.